

Geometry-Based Channel Estimation, Prediction, and Fusion

Benjamin J. B. Deutschmann¹, Erik Leitinger¹, and Klaus Witrisal¹

¹Graz University of Technology, Graz, Austria

Corresponding author: Benjamin J. B. Deutschmann (email: benjamin.deutschmann@tugraz.at).

The AMBIENT-6G project has received funding from the Smart Networks and Services Joint Undertaking (SNS JU) under the European Union's Horizon Europe research and innovation programme under Grant Agreement No. 101192113.

ABSTRACT Reciprocity-based beamforming—most commonly employed in time-division duplexing—uses noisy, estimated (i.e., measured) channel state information (CSI) acquired on the uplink. While computationally efficient, reciprocity-based beamforming suffers severe losses under (i) low signal-to-noise ratio (SNR) and (ii) user mobility because it ignores the underlying physics of the radio channel beyond its reciprocity. Based on a physics-driven geometry-based channel model, we propose a method that jointly infers the mobile user's position and environment map on the uplink. It then leverages the estimated user position and environment map to predict CSI on the downlink. We demonstrate significant efficiency gains under both (i) low SNR and (ii) user mobility on measured data. While the user position may allow efficient beamforming in strong line-of-sight (LoS) channels, inferring an environment map allows bypassing obstructed LoS conditions using non-LoS beamforming via multipath components. We further propose “channel fusion,” a probabilistic (Bayesian) combination of estimated and predicted CSI, which increases the beamforming robustness, particularly when either source of CSI is unreliable. Notably, this approach shares similarities with the minimum mean square error (MMSE) channel estimator, with geometry-based prior parameters inferred from the data.

INDEX TERMS MMSE, channel estimation, prediction, fusion, direct positioning, mapping, beamforming

I. INTRODUCTION

CHANNEL estimates acquired on the uplink (UL) are among the most commonly employed channel state information (CSI) for downlink (DL) beamforming (i.e., reciprocity-based beamforming) in time-division duplexing [1]. Channel prediction finds applications in “extrapolating” CSI to time or frequency points where observations have not been made [2]. Prominent examples include predicting future CSI to mitigate CSI aging under user mobility [3], or predictions from CSI observed on uplink frequencies to unobserved downlink frequencies in frequency-division duplexing [4]. We use the term “channel fusion” for methods that incorporate prior information to improve upon a noisy channel observation, or provide robustness if either the channel estimate or prior information are unreliable. To appreciate the terminology, consider a parametric multipath channel model [5]

$$\mathbf{h} = \Psi(\boldsymbol{\theta})\boldsymbol{\alpha} \quad (1)$$

that models K signal sources with amplitudes $\boldsymbol{\alpha} \in \mathbb{C}^{K \times 1}$ propagated over a dictionary $\Psi \in \mathbb{C}^{N \times K}$ that is parameter-

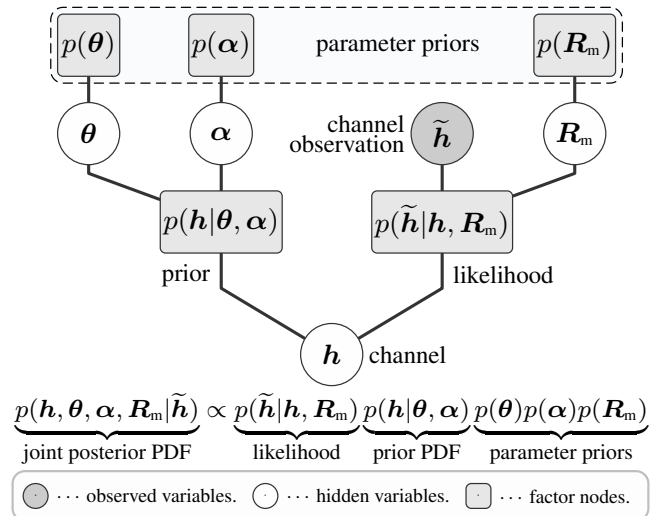


FIGURE 1: Factor graph representing channel fusion.

ized by a set of geometry-related parameters θ . With stochastic amplitudes $\alpha \sim p(\alpha)$ and parameters $\theta \sim p(\theta)$ the channel prior probability density function (PDF) is $p(\mathbf{h}|\theta, \alpha)$. Channel observations $\tilde{\mathbf{h}} = \mathbf{h} + \mathbf{n}$ are made in additive noise $\mathbf{n}|\mathbf{R}_m \sim \mathcal{CN}(\mathbf{0}, \mathbf{R}_m)$, hence the observation likelihood is $p(\tilde{\mathbf{h}}|\mathbf{h}, \mathbf{R}_m)$. The factor graph [6] in Fig. 1 represents the joint posterior distribution as the product of its factors. It can be shown to factorize (up to a proportionality constant) into a product of likelihood, prior, and parameter prior PDFs by exploiting the conditional independence structure that the factor graph makes explicit. We define the terminology:

- *Channel estimation*: Estimated CSI is computed through the maximum

$$\hat{\mathbf{h}}_m = \arg \max_{\mathbf{h}} (p(\tilde{\mathbf{h}}|\mathbf{h})) \triangleq \tilde{\mathbf{h}} \quad (2)$$

of the marginal likelihood $p(\tilde{\mathbf{h}}|\mathbf{h})$ and corresponds to the observed (i.e., measured) CSI $\tilde{\mathbf{h}}$.

- *Channel prediction*: Predicted CSI is computed through the expectation

$$\hat{\mathbf{h}}_p = \mathbb{E}(\mathbf{h}) \quad (3)$$

under the marginal prior PDF $p(\mathbf{h})$.

- *Channel fusion*: Fused CSI is computed through the expectation

$$\hat{\mathbf{h}}_f = \mathbb{E}(\mathbf{h}|\tilde{\mathbf{h}}) \quad (4)$$

under the marginal posterior PDF $p(\mathbf{h}|\tilde{\mathbf{h}}) \propto p(\tilde{\mathbf{h}}|\mathbf{h})p(\mathbf{h})$.

A prominent example of channel fusion is minimum mean square error (MMSE) channel estimation [7] which often assumes *known* prior parameters, meaning that the model parameters are replaced with constants. Suppose the parameters cannot be assumed known. There are two popular approximate but closed-form methods to treat the parameter prior PDFs for obtaining the marginal PDFs in (2)-(4) that evade a potentially expensive direct marginalization: Marginalization exploiting conjugate parameter priors [8, Sec. 2.4.2], or concentration at ML estimates of the parameters computed from the data (i.e., empirical Bayes) [9]. The literature on methods related to what we term channel fusion can be divided into categories that differ in how the channel prior PDF is modeled:

A. Model-based approaches:

- Models based on a geometry-agnostic channel prior $p(\mathbf{h})$ possibly inferring parameter priors online from the data [2], [9]–[12]. Prominent members of this category are works that first predict CSI (to future time steps) using an autoregressive model and then fuse it with estimated CSI using a Kalman filter directly in the space of the channel \mathbf{h} rather than the parameters θ [11], [12].
- Models based on a physics-driven geometry-based prior $p(\mathbf{h}|\theta, \alpha)$ where priors of geometry-related channel parameters $p(\theta)$ and amplitudes $p(\alpha)$ are inferred and tracked online to predict future CSI [2], [13].

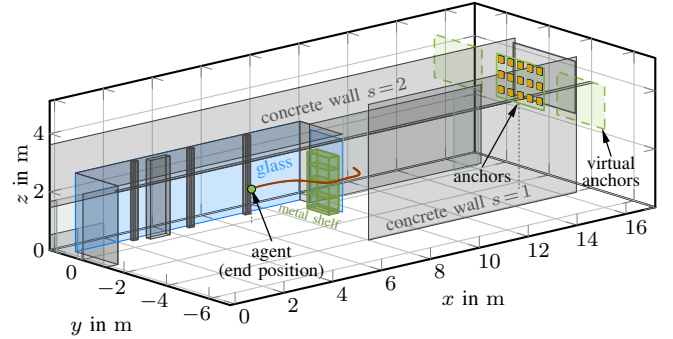


FIGURE 2: The measurement scenario: A mobile agent is moving on a trajectory around a shelf from LoS to OLOS conditions.

B. Data-driven approaches:

- Models based on a geometry-agnostic channel prior $p(\mathbf{h})$ learned offline from training data where geometry-related parameters enter only implicitly [12], [14], [15].
- Models based on a data-driven geometry-based prior $p(\mathbf{h}|\theta)$ with parameter prior $p(\theta)$ learned offline from the training data [16], [17].

This work belongs to category A.ii) where we devise a direct multipath-based simultaneous localization and mapping (SLAM) method [18], [19] that works directly on the radio signal (the observed CSI) to infer the multipath channel parameters θ and amplitudes α . State-of-the-art multipath-based SLAM methods assume an unknown model-order (i.e., number of sources K) and can be implemented in either a two-step approach, using a parametric channel estimation [20]–[24] algorithm followed by a multipath-based SLAM algorithm [25]–[31], or in a direct approach [18], [19], [32]. Leveraging the parameters inferred on the UL, our method demonstrates efficient CSI predictions on the DL under low signal-to-noise ratio (SNR) and user mobility, as well as robust positioning and CSI fusion even under line-of-sight (LoS) obstructions.

II. SCENARIO, METHOD, AND HYPOTHESES

Scenario. We perform i) UL positioning and mapping and ii) DL beamforming, where we evaluate our methods in a real-world hallway scenario schematically depicted in Fig. 2. We conduct synthetic aperture measurements with a mechanical positioner where we subsequently measure the channels between a mobile single-antenna agent and $J=15$ static anchors, each equipped with an (8×8) -uniform rectangular array (URA), that jointly form a *physically large* aperture, i.e., an aperture that is large w.r.t. the propagation distances of interest [33]. The anchors are assumed to be frequency synchronized through a shared reference clock and phase calibrated. A Rohde & Schwarz ZVA24 vector network analyzer (VNA) is used to measure the transmission coefficients, i.e., S-parameters, between a receiving anchor antenna m and the transmitting agent antenna [34]. We emulate to operate with a bandwidth of $B = 500$ MHz centered around $f_c = 6.175$ GHz which matches with the

new radio (NR) band n102, used for Wi-Fi 6E defined in IEEE Std. 802.11ax [35].

Method. The mobile agent transmits UL pilots while moving around a shelf filled with highly absorbing¹ material from strong LoS conditions into totally obstructed LoS (OLoS) conditions. On the UL, the J anchors acquire noisy channel observations—*estimated* CSI—which are used in our geometry-based *parametric* channel estimator to jointly infer the agent position and environment map. On the DL, efficient beamforming requires high-quality CSI. Conjugate beamforming [7] given estimated CSI, i.e., *reciprocity-based* beamforming, suffers both from i) *noisy* CSI estimates and from ii) CSI *aging* due to agent mobility.

Hypotheses.

- 1) **Robustness:** Robust and accurate positioning of the agent even in OLoS conditions is enabled through non-LoS (NLoS) components, i.e., rays that are reflected off walls, leveraging the previously learned environment map.
- 2) **Efficiency:** After being used for inference in the inverse problem of estimating geometric parameters from noisy estimated CSI, we leverage our geometry-based channel model to solve the forward problem of *predicting* CSI given the inferred agent position and environment map. Our geometry-based beamformer given predicted CSI can outperform a reciprocity-based beamformer given noisy CSI because it incorporates physics-based channel knowledge and rejects physically implausible CSI.
- 3) **Mobility Support:** We leverage a motion model to predict future agent positions and further predict CSI to future time steps, which gives our geometry-based beamformer the ability to perform efficiently even under user mobility where a conventional reciprocity-based beamformer given outdated CSI suffers from losses due to CSI aging.

III. SIGNAL MODEL

A. CHANNEL MODEL

We assume that at each time step $n \in \{1 \dots N\}$, each anchor $j \in \{1 \dots J\}$ acquires a noisy frequency-domain channel estimate

$$\tilde{\mathbf{h}}_{m,n,j} = \sum_{(s,s') \in \tilde{\mathcal{D}}} \mathbf{h}_{m,n,j}^{(s,s')} + \mathbf{w}_{m,n,j}^{\text{AWGN}} \in \mathbb{C}^{N_f \times 1} \quad (5)$$

per antenna $m \in \{1 \dots M\}$ in complex baseband with elements $[\tilde{\mathbf{h}}_{m,n,j}]_{n_f}$ and $n_f \in \{-\frac{N_f-1}{2} \dots \frac{N_f-1}{2}\}$ being discrete-frequency samples equally-spaced at $\Delta f = \frac{B}{N_f}$ and the number of frequency bins N_f either being an odd integer, or n_f being centered between two integers. Eq. (5) consists of two terms: The first term represents a sum of a LoS channel vector $\mathbf{h}_{m,n,j}^{(0,0)}$ and up to S^2 specular multipath component (SMC) channel vectors $\{\mathbf{h}_{m,n,j}^{(s,s')} | (s,s') \in \mathcal{D}\}$ modeling single-bounce reflections $(s,s) \in \mathcal{D}_S := \{(s,s) \in \mathcal{S} \times \mathcal{S}\}$ or double-bounce reflections $(s,s') \in \mathcal{D}_D := \{(s,s') \in \mathcal{S} \times \mathcal{S} | s \neq s'\}$ at large, planar surfaces $s \in \mathcal{S} := \{1 \dots S\}$, where $\mathcal{D} := \mathcal{D}_S \cup \mathcal{D}_D$ and $\tilde{\mathcal{D}} := (0,0) \cup \mathcal{D}$. The second term

represents an additive white Gaussian noise (AWGN) vector of N_f i.i.d. circular Gaussian noise samples $[\mathbf{w}_{m,n,j}^{\text{AWGN}}]_{n_f} \sim \mathcal{CN}(0, \sigma_j^2)$. Our inference channel model neglects diffuse multipath (DM) which typically represents stochastic scattering at small objects, or surfaces that are rough (w.r.t. the wavelength λ) [36]–[38].

The M noisy channel estimates are stacked into a matrix $\tilde{\mathbf{H}}_{n,j} = [\tilde{\mathbf{h}}_{1,n,j} \dots \tilde{\mathbf{h}}_{M,n,j}] \in \mathbb{C}^{N_f \times M}$ and vectorized to obtain the channel observation vector $\mathbf{z}_n^{(j)} = \text{vec}(\tilde{\mathbf{H}}_{n,j}) \in \mathbb{C}^{N_f M \times 1}$, which can be expressed in matrix-vector notation as

$$\mathbf{z}_n^{(j)} = \mathbf{\Psi}_j(\boldsymbol{\theta}_n) \boldsymbol{\alpha}_{n,j} + \mathbf{w}_n^{(j)}, \quad (6)$$

assuming temporally and spatially uncorrelated noise $\mathbf{w}_n^{(j)} \sim \mathcal{CN}(\mathbf{0}, \sigma_j^2 \mathbf{I}_{N_f M})$, and where $\mathbf{\Psi}_j(\boldsymbol{\theta}_n) = [\boldsymbol{\psi}_j^{(0,0)} \dots \boldsymbol{\psi}_j^{(s',s')}] \in \mathbb{C}^{N_f M \times K}$, parameterized² by a (random) state vector $\boldsymbol{\theta}_n$ capturing geometry-related parameters, is a dictionary matrix with $K := |\tilde{\mathcal{D}}| = S^2 + 1$ column-vectors $\boldsymbol{\psi}_j^{(s',s')}(\boldsymbol{\theta}_n) = \text{vec}(\mathbf{H}_{n,j}^{(s',s')})$. They are found as the vectorizations of the spatiotemporal array manifold $\mathbf{H}_{n,j}^{(s',s')} \in \mathbb{C}^{N_f \times M}$ with unit-modulus elements

$$[\mathbf{H}_{n,j}^{(s',s')}]_{n_f, m} = \exp\left(-j \frac{2\pi}{c} (f_c + \Delta f n_f) d_{m,n,j}^{(s',s')}\right) \quad (7)$$

parameterized on the path lengths $d_{m,n,j}^{(s',s')}(\boldsymbol{\theta}_n)$ that are a function of the state vector. The amplitudes $[\boldsymbol{\alpha}_{n,j}]_\kappa$ for one component $\kappa \in \{1 \dots K\}$ in (6) are assumed to be approximately constant over all antennas m of one anchor j and capture the lumped effects of direction-dependent antenna gains, distance-dependent path losses, losses due to impedance and polarization mismatch, as well as losses incurring due to reflections at specular surfaces [34], [39]. The important link between the array manifold and geometry is captured in the path lengths $d_{m,n,j}^{(s',s')}$ described by our geometric model, which we define next and which leads to our choice of $\boldsymbol{\theta}_n$.

B. LOS AND SPECULAR MULTIPATH MODEL

To describe the environment geometry, we use the master virtual anchor (MVA) model from [29] defining a specular surface s solely through the MVA position $\mathbf{p}_s^{\text{mva}}$, which is computed by mirroring the origin $\mathbf{0}$ of the global Cartesian coordinate system across surface s . It elegantly represents both the position of the surface through a wall-point

$$\mathbf{p}_s^{\text{w}} = \frac{\mathbf{p}_s^{\text{mva}}}{2} \in \mathbb{R}^{3 \times 1} \quad (8)$$

and the surface orientation through a normal vector

$$\mathbf{n}_s^{\text{w}} = \frac{\mathbf{p}_s^{\text{mva}}}{\|\mathbf{p}_s^{\text{mva}}\|} \in \mathbb{R}^{3 \times 1} \quad (9)$$

with only a single variable $\mathbf{p}_s^{\text{mva}} \in \mathbb{R}^{3 \times 1}$.

1) Physical Anchors

We define physical anchors (PAs) j centered around the phase center position $\mathbf{p}_{c,j}^{(0,0)} \in \mathbb{R}^{3 \times 1}$ with antennas m located at positions $\mathbf{p}_m^{\text{a}} \in \mathbb{R}^{3 \times 1}$ relative to $\mathbf{p}_{c,j}^{(0,0)}$. The complete “template” anchor array layout relative to $\mathbf{p}_{c,j}^{(0,0)}$ is captured in $\mathbf{P}_1 = [\mathbf{p}_1^{\text{a}} \dots \mathbf{p}_M^{\text{a}}] \in \mathbb{R}^{3 \times M}$ and is identical for all

¹Pyramidal absorbers are used to cause a strong obstruction.

²The dependence of $\mathbf{\Psi}_j$ on $\boldsymbol{\theta}_n$ is frequently omitted for notational brevity.

anchors. The antenna positions of an actual *physical* anchor are computed by shifting a “*template*” anchor out of the origin $\mathbf{0}$ to its center position $\mathbf{p}_{c,j}^{(0,0)}$ in global coordinates through

$$\mathbf{P}_j^{(0,0)} = \mathbf{p}_{c,j}^{(0,0)} \mathbf{1}_{1 \times M} + \mathbf{M}_j \mathbf{P}_t \in \mathbb{R}^{3 \times M}, \quad (10)$$

where $\mathbf{1}_{i \times j}$ denotes an $(i \times j)$ -matrix of all ones. The matrix $\mathbf{M}_j \in \mathbb{R}^{3 \times 3}$ is a rotation matrix that defines the orientation of PA j in global coordinates.

2) Single-Bounce Virtual Anchors

Reflections of the agent’s UL pilots at large specular surfaces are modeled as if they were virtually impinging at virtual anchors (VAs) that are images of PAs mirrored across surfaces s . We model VAs using MVAs as described in [29]: The transformation from a PA to a VA phase center position is computed using the function $h_{va} : \mathbb{R}^3 \times \mathbb{R}^3 \rightarrow \mathbb{R}^3$ defined as

$$\begin{aligned} \mathbf{p}_{c,j}^{(s,s)} &= h_{va}(\mathbf{p}_{c,j}^{(0,0)}, \mathbf{p}_s^{mva}) \\ &= \mathbf{p}_{c,j}^{(0,0)} - \left(\frac{2 \mathbf{p}_{c,j}^{(0,0)\top} \mathbf{p}_s^{mva}}{\|\mathbf{p}_s^{mva}\|^2} - 1 \right) \mathbf{p}_s^{mva}. \end{aligned} \quad (11)$$

The Householder matrix

$$\mathcal{H}_s = \mathbf{I}_3 - 2 \frac{\mathbf{p}_s^{mva} \mathbf{p}_s^{mva\top}}{\|\mathbf{p}_s^{mva}\|^2} \quad (12)$$

represents the transformation from the PA orientation to the VA orientation when mirrored across specular surface s . The complete array layout of a single-bounce VA is captured in

$$\mathbf{P}_j^{(s,s)} = \mathbf{p}_{c,j}^{(s,s)} \mathbf{1}_{1 \times M} + \mathcal{H}_s \mathbf{M}_j \mathbf{P}_t \in \mathbb{R}^{3 \times M}. \quad (13)$$

3) Double-Bounce Virtual Anchors

As described in [29], a double-bounce VA phase center position is computed by applying (11) twice, i.e., $\mathbf{p}_{c,j}^{(s,s')} = h_{va}(h_{va}(\mathbf{p}_{c,j}^{(0,0)}, \mathbf{p}_s^{mva}), \mathbf{p}_{s'}^{mva})$. The orientation transformation of the double bounce path (s, s') is taken into account by applying Householder matrices \mathcal{H}_s and $\mathcal{H}_{s'}$ from both surfaces using (12), which leads to the representation of the complete array layout of a double-bounce VA in global coordinates as

$$\mathbf{P}_j^{(s,s')} = \mathbf{p}_{c,j}^{(s,s')} \mathbf{1}_{1 \times M} + \mathcal{H}_{s'} \mathcal{H}_s \mathbf{M}_j \mathbf{P}_t \in \mathbb{R}^{3 \times M}. \quad (14)$$

Linking our geometric model to the array manifold in (7), the path lengths

$$d_{m,n,j}^{(s,s')} = \|\mathbf{p}_{m,j}^{(s,s')} - \mathbf{p}_n\| \quad (15)$$

are the scalar distances from the agent at $\mathbf{p}_n \in \mathbb{R}^{3 \times 1}$ to the receiving antenna positions $\mathbf{p}_{m,j}^{(s,s')}$ captured³ in the layout for PAs in (10), for single-bounce VAs in (13), and for double-bounce VAs in (14).

C. Problem Formulation

In the *inverse* problem, we aim to infer the geometry-based channel parameters, i.e., the state θ_n , that led to the data, i.e., the anchor infrastructure observations $\mathbf{Z}_n := [\mathbf{z}_1^{(n)} \dots \mathbf{z}_J^{(n)}] \in \mathbb{C}^{N_f M \times J}$. We choose a joint state vector

$$\theta_n = [\mathbf{x}_n^\top, \bar{\mathbf{p}}^{mva\top}]^\top \in \mathcal{S}_\theta, \quad (16)$$

with $\mathcal{S}_\theta = \mathbb{R}^{5+3S}$ denoting the state space, which comprises the agent state \mathbf{x}_n and the stacked MVA state $\bar{\mathbf{p}}^{mva}$. The agent state $\mathbf{x}_n = [\mathbf{p}_n^\top, \mathbf{v}_n^\top]^\top \in \mathbb{R}^{5 \times 1}$ contains the three-dimensional agent position $\mathbf{p}_n \in \mathbb{R}^{3 \times 1}$, but only a horizontal agent velocity $\mathbf{v}_n \in \mathbb{R}^{2 \times 1}$ as the agent has no vertical motion. Capturing the map information, the stacked MVA state $\bar{\mathbf{p}}^{mva} = [\mathbf{p}_1^{mva\top} \dots \mathbf{p}_S^{mva\top}]^\top \in \mathbb{R}^{3S \times 1}$ solely comprises the MVA positions in this work, although it could be extended to track the existence of a surface [29], or parameters describing its reflective properties.

In the *forward* problem, we aim to predict the data, i.e., a channel vector $\mathbf{h}_{n,j}^p$, parameterized by our estimated parameters $\hat{\theta}_n$. Our methods to solve the inverse and forward problems are found in Sec. IV and Sec. VI, respectively.

IV. SPATIAL-DELAY POSITIONING AND MAPPING

To fuse the information on the state acquired on subsequent observations, we employ the Bayesian filtering equation [40]

$$p(\theta_n | \mathbf{Z}_{1:n}) = \frac{p(\mathbf{Z}_n | \theta_n) p(\theta_n | \mathbf{Z}_{1:n-1})}{p(\mathbf{Z}_n | \mathbf{Z}_{1:n-1})} \quad (17)$$

that describes the posterior PDF $p(\theta_n | \mathbf{Z}_{1:n})$ of the state vector θ_n at time step n given past observations (i.e., measurements) $\mathbf{Z}_{1:n-1} := \{\mathbf{Z}_1, \dots, \mathbf{Z}_{n-1}\}$ and the current observation \mathbf{Z}_n . Assuming a first-order Markov chain, i.e., $p(\theta_n | \theta_{n-1} \dots \theta_0) = p(\theta_n | \theta_{n-1})$, the prediction PDF $p(\theta_n | \mathbf{Z}_{1:n-1})$ is computed from the state-transition PDF and the previous posterior PDF through the Chapman-Kolmogorov equation

$$p(\theta_n | \mathbf{Z}_{1:n-1}) = \int_{\mathcal{S}_\theta} p(\theta_n | \theta_{n-1}, \mathbf{Z}_{1:n-1}) p(\theta_{n-1} | \mathbf{Z}_{1:n-1}) d\theta_{n-1}$$

where we assume that the state-transition PDF $p(\theta_n | \theta_{n-1}, \mathbf{Z}_{1:n-1}) = p(\theta_n | \theta_{n-1}) := \mathcal{N}(\Phi \theta_{n-1}, \mathbf{Q})$ is defined through the state-space model

$$\theta_n = \Phi \theta_{n-1} + \omega_n \quad (18)$$

where $\omega_n \in \mathcal{S}_\theta$ denotes zero-mean Gaussian process noise with a diagonal covariance matrix $\mathbf{Q} := \text{diag}(\sigma_p^2, \sigma_p^2, \sigma_p^2, \sigma_v^2, \sigma_v^2, \sigma_{mva}^2 \dots \sigma_{mva}^2)$ and Φ is a state-transition matrix defined as

$$[\Phi]_{k,\ell} = \begin{cases} 1 & k = \ell \\ \Delta t & ((k, \ell) = (1, 4)) \vee ((k, \ell) = (2, 5)) \\ 0 & \text{else,} \end{cases} \quad (19)$$

with Δt denoting the time interval between two subsequent observations \mathbf{Z}_{n-1} and \mathbf{Z}_n . In Sec. V we define two models for the likelihood $p(\mathbf{Z}_n | \theta_n)$ of the observation conditional on the state.

We approximately implement (17) through a particle filter (PF) with a *random measure* $\{\theta_n^{(i)}, w_{n|n}^{(i)}\}_{i=1}^{N_p}$ of N_p particles $\theta_n^{(i)}$ with weights $w_{n|n}^{(i)}$ s.t. $\sum_{i=1}^{N_p} w_{n|n}^{(i)} \triangleq 1$, implicitly accounting for the normalization constant $p(\mathbf{Z}_n | \mathbf{Z}_{1:n-1})$. The PF approximates the posterior PDF as $\hat{p}(\theta_n | \mathbf{Z}_{1:n}) = \sum_{i=1}^{N_p} w_{n|n}^{(i)} \delta(\theta_n - \theta_n^{(i)})$ from which we estimate the state θ_n by approximating the MMSE estimate $\theta_n^{\text{MMSE}} = \mathbb{E}(\theta_n | \mathbf{Z}_{1:n})$

³Position $\mathbf{p}_{m,j}^{(s,s')}$ is the m^{th} column vector in the respective layout.

as

$$\hat{\theta}_n = \int_{\mathfrak{S}_\theta} \theta_n \hat{p}(\theta_n | \mathbf{Z}_{1:n}) d\theta_n = \sum_{i=1}^{N_p} \theta_n^{(i)} w_{n|n}^{(i)}, \quad (20)$$

and approximate the state covariance matrix as

$$\hat{\mathbf{P}}_n = \sum_{i=1}^{N_p} \left(\theta_n^{(i)} - \hat{\theta}_n \right) \left(\theta_n^{(i)} - \hat{\theta}_n \right)^\top w_{n|n}^{(i)}. \quad (21)$$

We use a regularized PF, implemented through [41, Alg. 1] by replacing the likelihood function in line 6 with the stochastic likelihood function implemented by Alg. 1 below.

V. LIKELIHOOD MODEL

A. DETERMINISTIC CONCENTRATED LIKELIHOOD

The statistical model of the observations $\mathbf{z}_n^{(j)}$ in (6) underlying the deterministic concentrated likelihood [42] assumes that the signal amplitudes $\alpha_{n,j}$ are *deterministic* unknowns. Per (6), the per-anchor observation is distributed as $\mathbf{z}_n^{(j)} | \theta_n \sim \mathcal{CN}(\Psi_j(\theta_n) \alpha_{n,j}, \sigma_j^2 \mathbf{I}_{N_f M})$. Assuming independent observations among all anchors j leaves us with the deterministic likelihood function

$$p(\mathbf{Z}_n; \theta_n, \{\alpha_{n,j}\}_{j=1}^J, \{\sigma_j^2\}_{j=1}^J) = \prod_{j=1}^J \frac{\exp\left(-\frac{1}{\sigma_j^2} \|\mathbf{z}_n^{(j)} - \Psi_j(\theta_n) \alpha_{n,j}\|^2\right)}{(\pi \sigma_j^2)^{N_f M}} \quad (22)$$

for the infrastructure observation \mathbf{Z}_n parameterized by the state θ_n , the amplitudes $\{\alpha_{n,j}\}_{j=1}^J$, and noise variances $\{\sigma_j^2\}_{j=1}^J$. Since the latter two contribute negligible information about the state θ_n , we treat them as nuisance parameters and we compute the *profile* likelihood, i.e., we *concentrate* w.r.t. the nuisance parameters by computing maximum likelihood (ML) estimates conditional on the state θ_n . ML estimates of amplitudes are found as

$$\hat{\alpha}_{n,j} | \theta_n = \Psi_j^\dagger \mathbf{z}_n^{(j)}, \quad (23)$$

with $\Psi_j^\dagger(\theta_n)$ denoting the pseudoinverse of the dictionary, while ML estimates of noise variances are computed as [42, eq. (48)]

$$\hat{\sigma}_j^2 | \theta_n = \frac{1}{N_f M} \text{tr} \left(\Pi_j^\perp \hat{\mathbf{R}}_{n,j}^e \right) \quad (24)$$

with $\Pi_j^\perp(\theta_n) = \mathbf{I}_{N_f M} - \Psi_j \Psi_j^\dagger$ being the projector onto the noise subspace, i.e., the orthogonal complement of the subspace spanned by $\Psi_j(\theta_n)$, and the sample covariance matrix $\hat{\mathbf{R}}_{n,j}^e := \mathbf{z}_n^{(j)} \mathbf{z}_n^{(j)H}$ is an *empirical* rank-1 estimate of the spatiotemporal signal covariance matrix $\mathbf{R}_{n,j} = \mathbb{E}(\mathbf{z}_n^{(j)} \mathbf{z}_n^{(j)H})$. Despite notationally brief, (24) is computationally expensive and can be implemented efficiently using (40) in Appendix C. Reinsertion of $\hat{\alpha}_{n,j} | \theta_n$ and $\hat{\sigma}_j^2 | \theta_n$ in (22) yields the deterministic profile likelihood function⁴

$$p(\mathbf{Z}_n | \theta_n) = \prod_{j=1}^J \frac{\exp\left(-\frac{1}{\hat{\sigma}_j^2} \|\Pi_j^\perp \mathbf{z}_n^{(j)}\|^2\right)}{(\pi \hat{\sigma}_j^2)^{N_f M}}. \quad (25)$$

⁴Note that $\mathbf{z}_n^{(j)} - \Psi_j \hat{\alpha}_{n,j} \triangleq \Pi_j^\perp \mathbf{z}_n^{(j)}$ and (40) omit computing Π_j^\perp .

B. STOCHASTIC CONCENTRATED LIKELIHOOD

The statistical model of the observations $\mathbf{z}_n^{(j)}$ in (6) underlying the stochastic concentrated likelihood [43] assumes that the signal amplitudes are *stochastic* unknowns with prior PDF $p(\alpha_{n,j} | \mu_{n,j}, \mathbf{P}_{n,j}) = \mathcal{CN}(\mu_{n,j}, \mathbf{P}_{n,j})$ parameterized by an unknown source covariance matrix $\mathbf{P}_{n,j} \in \mathbb{C}^{K \times K}$. Contrary to the established definition in the literature, we define amplitudes to have an unknown mean $\mu_{n,j} \neq \mathbf{0}$, yet in Appendix A we show that the established ML estimators are still unbiased in concentrating the likelihood in (26) w.r.t. the nuisance parameters. It follows per (6) that the per-anchor observation is distributed as $\mathbf{z}_n^{(j)} | \theta_n \sim \mathcal{CN}(\Psi_j(\theta_n) \mu_{n,j}, \mathbf{R}_{n,j})$ with the spatiotemporal signal covariance matrix $\mathbf{R}_{n,j} = \Psi_j \mathbf{P}_{n,j} \Psi_j^H + \sigma_j^2 \mathbf{I}_{N_f M}$. Assuming independent observations among all anchors j leaves us with the stochastic likelihood function

$$p(\mathbf{Z}_n | \theta_n, \{\mu_{n,j}\}_{j=1}^J, \{\mathbf{R}_{n,j}\}_{j=1}^J) = \prod_{j=1}^J \frac{\exp\left(-(\mathbf{z}_n^{(j)} - \Psi_j(\theta_n) \mu_{n,j})^H \mathbf{R}_{n,j}^{-1} (\mathbf{z}_n^{(j)} - \Psi_j(\theta_n) \mu_{n,j})\right)}{\pi^{N_f M} |\mathbf{R}_{n,j}|} \quad (26)$$

for the infrastructure observation \mathbf{Z}_n . Again, we compute the profile likelihood by concentrating w.r.t. the nuisance parameters, using the ML estimators (cf. [42], [43])

$$\hat{\alpha}_{n,j} | \theta_n = \Psi_j^\dagger \mathbf{z}_n^{(j)}, \quad (27)$$

$$\hat{\sigma}_j^2 | \theta_n = \frac{1}{N_f M - K} \text{tr} \left(\Pi_j^\perp \hat{\mathbf{R}}_{n,j}^e \right), \quad (28)$$

$$\hat{\mathbf{P}}_{n,j} | \theta_n = \Psi_j^\dagger \left(\hat{\mathbf{R}}_{n,j}^e - \hat{\sigma}_j^2 \mathbf{I}_{N_f M} \right) \Psi_j^{\dagger H}, \quad (29)$$

with which we define a refined estimate $\hat{\mathbf{R}}_{n,j} | \theta_n := \Psi_j \hat{\mathbf{P}}_{n,j} \Psi_j^H + \hat{\sigma}_j^2 \mathbf{I}_{N_f M}$ that, reinserted in (26), yields the stochastic profile likelihood function

$$p(\mathbf{Z}_n | \theta_n) = \prod_{j=1}^J \frac{\exp\left(-\left\| \hat{\mathbf{R}}_{n,j}^{-\frac{1}{2}} (\mathbf{z}_n^{(j)} - \Psi_j(\theta_n) \hat{\alpha}_{n,j}) \right\|^2\right)}{\pi^{N_f M} |\hat{\mathbf{R}}_{n,j}|} \quad (30)$$

assuming $\hat{\mathbf{R}}_{n,j} | \theta_n$ to be positive definite. Despite notationally brief, (30) is computationally expensive and can be implemented efficiently using (41) and (42) from Appendix C.

VI. CHANNEL ESTIMATION, PREDICTION, AND FUSION

In the forward problem, we aim to predict data, i.e., a channel vector $\mathbf{h}_{n,j}^p$, given the estimated parameters, i.e., the state estimate $\hat{\theta}_n$. In this work, we evaluate channel prediction only at the carrier frequency f_c , i.e., we henceforth use $N_f = 1$ for prediction.⁵ Under the assumption of frequency synchrony, we perform coherent joint transmission (CJT) with all J anchors, although we discuss CSI estimation, prediction, and fusion only for a single anchor j . For notational brevity, we omit the conditioning on $\mathbf{Z}_{1:n}$ for the remainder of this section.

⁵We keep the notation of the preceding sections, assuming that the quantities are respectively scaled in dimensions.

Algorithm 1: Concentrated Stochastic Likelihood

Input : Observation \mathbf{Z}_n , particle $\theta_n^{(i)}$
Output: Unnormalized weight $\tilde{w}_n^{(i)} \leftarrow p(\mathbf{Z}_n | \theta_n^{(i)})$

- 1 $\mathbf{p}_n \leftarrow [\theta_n^{(i)}]_{1:3}$, $\bar{\mathbf{p}}^{mva} \leftarrow [\theta_n^{(i)}]_{6:5+3S}$, and $\tilde{w}_n^{(i)} \leftarrow 0$
- 2 **for** $j \leftarrow 1$ **to** J **by** 1 **do**
- 3 $\Psi_j \leftarrow \mathbf{0}$ and $\kappa \leftarrow 1$
- 4 $[\Psi_j]_{:, \kappa} \leftarrow \text{psi}(\mathbf{p}_n, \mathbf{p}_{c,j}^{(0,0)}, \mathbf{P}_t, \mathbf{I}_3, \mathbf{I}_3)$
- 5 **for** $s \leftarrow 1$ **to** S **by** 1 **do**
- 6 $\{\mathbf{p}_{c,j}^{(s,s)}, \mathcal{H}_s\} \leftarrow \text{computeVA}(\mathbf{p}_{c,j}^{(0,0)}, \mathbf{p}_s^{mva})$
- 7 **for** $s' \leftarrow 1$ **to** S **by** 1 **do**
- 8 $\kappa \leftarrow \kappa + 1$
- 9 **if** $s = s'$ **then**
- 10 $[\Psi_j]_{:, \kappa} \leftarrow \text{psi}(\mathbf{p}_n, \mathbf{p}_{c,j}^{(s,s)}, \mathbf{P}_t, \mathcal{H}_s, \mathbf{I}_3)$
- 11 **else**
- 12 $\{\mathbf{p}_{c,j}^{(s,s')}, \mathcal{H}_{s'}\} \leftarrow \text{computeVA}(\mathbf{p}_{c,j}^{(s,s)}, \mathbf{p}_{s'}^{mva})$
- 13 $[\Psi_j]_{:, \kappa} \leftarrow \text{psi}(\mathbf{p}_n, \mathbf{p}_{c,j}^{(s,s')}, \mathbf{P}_t, \mathcal{H}_s, \mathcal{H}_{s'})$
- 14 **end**
- 15 **end**
- 16 **end**
- 17 $\hat{\mathbf{R}}_{n,j}^e \leftarrow \mathbf{z}_n^{(j)} \mathbf{z}_n^{(j)H}$
- 18 $\hat{\alpha}_{n,j} | \theta_n^{(i)} \leftarrow \Psi_j^\dagger \mathbf{z}_n^{(j)} \quad // \text{see (27)}$
- 19 $\hat{\sigma}_j^2 | \theta_n^{(i)} \leftarrow \frac{1}{N_f M - K} \text{tr}(\Pi_j^\perp \hat{\mathbf{R}}_{n,j}^e) \quad // (28) \text{ using (40)}$
- 20 $\hat{\mathbf{P}}_{n,j} | \theta_n^{(i)} \leftarrow \Psi_j^\dagger (\hat{\mathbf{R}}_{n,j}^e - \hat{\sigma}_j^2 \mathbf{I}_{N_f M}) \Psi_j^{iH} \quad // \text{see (38)}$
- 21 $\tilde{w}_n^{(i)} \leftarrow \tilde{w}_n^{(i)} \times p(\mathbf{z}_n^{(j)} | \theta_n^{(i)}) \quad // (26) \text{ using (41), (42)}$
- 22 **end**
- 23 **Sub-routine** $\psi_j^{(s,s')} \leftarrow \text{psi}(\mathbf{p}_n, \mathbf{p}_{c,j}^{(s,s')}, \mathbf{P}_t, \mathcal{H}_s, \mathcal{H}_{s'})$
- 25 $\mathbf{P}_j^{(s,s')} \leftarrow \mathbf{p}_{c,j}^{(s,s')} \mathbf{1}_{1 \times M} + \mathcal{H}_{s'} \mathcal{H}_s M_j \mathbf{P}_t \quad // \text{see (14)}$
- 26 $\mathbf{d} \leftarrow \text{vecnorm}(\mathbf{P}_j^{(s,s')})^\top \quad // (M \times 1) \text{ distances}$
- 27 $\mathbf{H}_{n,j}^{(s,s')} \leftarrow \exp\left(-j \frac{2\pi}{c} (f_c \mathbf{1}_{N_f \times 1} + \mathbf{f}) \mathbf{d}^\top\right) \quad // \text{see (7)*}$
- 28 $\psi_j^{(s,s')} \leftarrow \text{vec}(\mathbf{H}_{n,j}^{(s,s')})$
- 29 **Sub-routine** $\{\mathbf{p}_{c,j}^{(s,s)}, \mathcal{H}_s\} \leftarrow \text{computeVA}(\mathbf{p}_{c,j}^{(0,0)}, \mathbf{p}_s^{mva})$
- 31 $\mathbf{p}_{c,j}^{(s,s)} \leftarrow \mathbf{p}_{c,j}^{(0,0)} - (2\mathbf{p}_{c,j}^{(0,0)\top} \mathbf{p}_s^{mva} / \|\mathbf{p}_s^{mva}\|^2 - 1) \mathbf{p}_s^{mva}$
 $// \text{see (11)}$
- 32 $\mathcal{H}_s \leftarrow \mathbf{I}_3 - 2\mathbf{p}_s^{mva} \mathbf{p}_s^{mva\top} / \|\mathbf{p}_s^{mva}\|^2 \quad // \text{see (12)}$

*To be understood as element-wise extension of the exponential function with $\mathbf{f} \in \mathbb{R}^{N_f \times 1}$ denoting the baseband frequency vector.

Estimated CSI. Stacking the M noisy channel estimates of anchor j into a vector $\tilde{\mathbf{h}}_{n,j} = [\tilde{h}_{1,n,j} \dots \tilde{h}_{M,n,j}]^\top \in \mathbb{C}^{M \times 1}$, estimated CSI is obtained which satisfies $\tilde{\mathbf{h}}_{n,j} = \arg \max_{\mathbf{h}_{n,j}} (p(\tilde{\mathbf{h}}_{n,j} | \mathbf{h}_{n,j}, \sigma_j^2))$.

Predicted CSI. Concentrating the channel prior PDF $p(\mathbf{h}_{n,j} | \theta_n, \alpha_{n,j})$ with $\hat{\alpha}_{n,j} | \theta_n$ from (27) at the state estimate $\hat{\theta}_n$, we compute predicted CSI as

$$\mathbf{h}_{n,j}^p := \mathbb{E}(\mathbf{h}_{n,j}) = \Psi_j(\hat{\theta}_n) \hat{\alpha}_{n,j} \in \mathbb{C}^{M \times 1}. \quad (31)$$

Fused CSI. The observed vector $\tilde{\mathbf{h}}_{n,j}$ of estimated CSI is described through the likelihood $p(\tilde{\mathbf{h}}_{n,j} | \mathbf{h}_{n,j}, \sigma_j^2) = \mathcal{CN}(\mathbf{h}_{n,j}, \sigma_j^2 \mathbf{I}_M)$, i.e., corresponding to true CSI $\mathbf{h}_{n,j}$ observed in spatially uncorrelated circular AWGN with per-antenna noise variance σ_j^2 . Our predicted CSI $\mathbf{h}_{n,j}^p$ enters as the mean of the prior PDF $p(\mathbf{h}_{n,j} | \theta_n, \alpha_{n,j}) = \mathcal{CN}(\Psi_j(\theta_n) \boldsymbol{\mu}_{n,j}, \Psi_j \mathbf{P}_{n,j} \Psi_j^H)$ after concentration. Now we

seek the data fusion, i.e., the fused CSI $\mathbf{h}_{n,j}^f := \mathbb{E}(\mathbf{h}_{n,j} | \tilde{\mathbf{h}}_{n,j})$, computed from the posterior PDF (where conditional independences from Fig. 1 hold)

$$p(\mathbf{h}_{n,j} | \tilde{\mathbf{h}}_{n,j}, \theta_n, \alpha_{n,j}, \sigma_j^2) = \frac{p(\mathbf{h}_{n,j}, \tilde{\mathbf{h}}_{n,j} | \theta_n, \alpha_{n,j}, \sigma_j^2)}{p(\tilde{\mathbf{h}}_{n,j} | \theta_n, \alpha_{n,j}, \sigma_j^2)} \propto p(\tilde{\mathbf{h}}_{n,j} | \mathbf{h}_{n,j}, \sigma_j^2) p(\mathbf{h}_{n,j} | \theta_n, \alpha_{n,j}) \quad (32)$$

through concentration at $\hat{\theta}_n$, where our (profile) likelihood becomes $p(\tilde{\mathbf{h}}_{n,j} | \mathbf{h}_{n,j}) = \mathcal{CN}(\mathbf{h}_{n,j}, \hat{\sigma}_j^2 \mathbf{I}_M)$ and our (profile) prior PDF becomes $p(\mathbf{h}_{n,j}) = \mathcal{CN}(\Psi_j(\hat{\theta}_n) \hat{\alpha}_{n,j}, \Psi_j \hat{\mathbf{P}}_{n,j} \Psi_j^H)$. Given the product of the circular Gaussian likelihood and circular Gaussian prior PDF in (32), fused CSI is found as the posterior mean [44, Sec. 8.1.8]

$$\mathbf{h}_{n,j}^f = \mathbb{E}(\mathbf{h}_{n,j} | \tilde{\mathbf{h}}_{n,j}) = \mathbf{R}_{i,n,j} (\mathbf{R}_{m,n,j}^{-1} \tilde{\mathbf{h}}_{n,j} + \mathbf{R}_{p,n,j}^{-1} \mathbf{h}_{n,j}^p) \quad (33)$$

of $\mathbf{h}_{n,j} | \tilde{\mathbf{h}}_{n,j}$ which is likewise circular Gaussian-distributed (up to a normalization constant) with covariance matrix $\mathbf{R}_{i,n,j} = (\mathbf{R}_{m,n,j}^{-1} + \mathbf{R}_{p,n,j}^{-1})^{-1}$ and is found as the probabilistic data fusion of estimated CSI with covariance matrix $\mathbf{R}_{m,n,j} = \hat{\sigma}_j^2 \mathbf{I}_M$ and predicted CSI with covariance matrix $\mathbf{R}_{p,n,j} = \Psi_j \hat{\mathbf{P}}_{n,j} \Psi_j^H$. Due to $\text{rank}(\Psi_j \hat{\mathbf{P}}_{n,j} \Psi_j^H) \leq K \ll M$, (33) suffers from $\mathbf{R}_{p,n,j}$ being singular and hence $\mathbf{R}_{p,n,j}^{-1}$ does not exist.

Proposition 1. The channel fusion in (33) corresponds to the linear MMSE (LMMSE) estimator [45, Theorem 10.3]⁶

$$\mathbf{h}_{n,j}^f = \mathbf{h}_{n,j}^p + \mathbf{R}_{p,n,j} (\hat{\sigma}_j^2 \mathbf{I}_M + \mathbf{R}_{p,n,j})^{-1} (\tilde{\mathbf{h}}_{n,j} - \mathbf{h}_{n,j}^p). \quad (34)$$

Proof:

See Appendix B. ■

Using (34) instead of (33) allows the computation of $\mathbf{h}_{n,j}^f$ even with rank-deficient $\mathbf{R}_{p,n,j}$. Again, the inverse in (34) is efficiently implemented using (42).

VII. RESULTS

Given the scenario in Fig. 2, we choose a fixed model order, i.e., a constant state-vector dimension, representing only $S = 2$ planar surfaces (MVAs), i.e., $\bar{\mathbf{p}}^{mva} = [\mathbf{p}_1^{mva\top}, \mathbf{p}_2^{mva\top}]^\top$.

Experiment A. Inverse Problem

Our PF is initialized by drawing $N_p = 1000$ particles from $\mathcal{U}(\theta_{\min}, \theta_{\max})$ and given the observations $\{\mathbf{Z}_n\}_{n=1}^N$. We initialize by drawing particles uniformly from the spatial region between $[\theta_{\min}]_{1:3} = [4, -4, 0]^\top \text{m}$ and $[\theta_{\max}]_{1:3} = [12, 0, 3]^\top \text{m}$, covering the chosen scenario. We perform 1000 estimation runs with random particles $\{\theta_n^{(i)}\}_i^{N_p}$ and random noise $\mathbf{w}_n^{(j)} \sim \mathcal{CN}(\mathbf{0}, \sigma_j^2 \mathbf{I}_{N_f M})$ in each trajectory step, where we set the (time-constant) noise power $\sigma_j^2 = \sigma_j^2, \forall j, j' \in \{1 \dots J\}$

⁶Formulated for amplitudes α , the LMMSE estimator $\mathbb{E}(\alpha | \theta, \tilde{\mathbf{h}})$ in [45] needs to be left-multiplied by $\Psi(\theta)$ and concentrated using $\hat{\alpha} | \theta, \hat{\mathbf{P}} | \theta$ to result in $\mathbb{E}(\mathbf{h} | \theta, \tilde{\mathbf{h}}) = \Psi \hat{\alpha} + \Psi \hat{\mathbf{P}} \Psi^H (\sigma^2 \mathbf{I} + \Psi \hat{\mathbf{P}} \Psi^H)^{-1} (\tilde{\mathbf{h}} - \Psi \hat{\alpha})$, which is equivalent to (34), a common result in the literature [9], [10].

to satisfy $\text{SNR}(n=1) = -6$ dB at time $n=1$, which decreases $\text{SNR}(n) < -6$ dB for $n \gg 1$ due to the distance-dependent path loss and OLoS conditions. Here, SNR denotes the channel (input) SNR [34] which we define as $\text{SNR}(n) = \frac{1}{J} \sum_{j=1}^J \frac{\|\mathbf{h}_{n,j}\|^2/M}{\sigma_s^2}$. We only utilize $N_f = 6$ subcarrier frequencies equally spaced across the bandwidth B centered around f_c to perform channel estimation in the inverse problem. Fig. 3 shows the estimated trajectories $\{\hat{\mathbf{p}}_n\}_{n=1}^N$ (—) in comparison to the ground truth $\{\mathbf{p}_n\}_{n=1}^N$ (—). Fig. 4 shows the cumulative frequency of the horizontal position error $\|\hat{\mathbf{p}}_n\|_{1,2} - \|\mathbf{p}_n\|_{1,2}\|$ (—) and the vertical position error $\|\hat{\mathbf{p}}_n\|_3 - \|\mathbf{p}_n\|_3\|$ (—) over all N time steps of all 1000 realizations. After convergence, our estimator achieves an overall horizontal position root mean square error (RMSE) of 6.37 cm (—) and vertical position RMSE of 4.92 cm (—) using the stochastic likelihood in (30). Using the deterministic likelihood in (25), the RMSEs become 6.54 cm and 4.97 cm, respectively. As noted in the literature [42, p. 78], significant differences can be observed under low SNR, highly correlated signals, and small numbers of antennas, the latter of which is not the case in our scenario. Note, however, that (25) is computationally more efficient than (30). Using an LoS-only model, the performance degrades significantly both in the horizontal (---) and vertical (---) errors (41 cm and 8.4 cm RMSE).

Experiment B. Forward Problem

In Fig. 5 we evaluate the efficiency, i.e., the path gain (PG)⁷ $G(\{\hat{\mathbf{h}}_{n,j}\}_{j=1}^J) = \left| \sum_{j=1}^J \hat{\mathbf{h}}_{n,j}^H \mathbf{h}_{n,j} / \|\hat{\mathbf{h}}_{n,j}\| \right|^2$, of a conjugate beamformer, with $\hat{\mathbf{h}}_{n,j} \in \{\hat{\mathbf{h}}_{n,j}, \mathbf{h}_{n,j}^p, \mathbf{h}_{n,j}^f\}$ being any of our three types of estimated, predicted, or fused CSI: We have shown that the expected efficiency of a reciprocity-beamformer (—) given noisy estimated CSI $\hat{\mathbf{h}}_{n,j}$ incurs an efficiency loss⁸ of $\text{SNR}/(1+\text{SNR})$ w.r.t. perfect CSI [34, eq. (17)]. The realized efficiency $G(\{\hat{\mathbf{h}}_{n,j}\}_{j=1}^J) =: G_n^m$ depends on the actual noise realization, which is why we augment the expectation with a symmetric confidence interval $U_{98\%}$ (—) for which one random realization of G_n^m is located within the interval $[\mathbb{E}\{G_n^m\} - U_{98\%}, \mathbb{E}\{G_n^m\} + U_{98\%}]$ with a confidence level of 98%, i.e., the probability $98\% = \mathbb{P}(\mathbb{E}\{G_n^m\} - U_{98\%} \leq G_n^m \leq \mathbb{E}\{G_n^m\} + U_{98\%})$. For $\text{SNR} \leq -6$ dB, the reciprocity-beamformer incurs a loss of ≥ 6.98 dB w.r.t. perfect CSI. Our geometry-based beamformer given predicted CSI (—) outperforms the reciprocity beamformer by 6.5 dB on average for the chosen SNR. Before convergence of our PF or under a model mismatch through e.g. assuming an LoS-only model under OLoS conditions as shown in Fig. 5 b), estimated CSI outperforms predicted CSI. The benefits of fused CSI (—) from (33) become evident when comparing Fig. 5 a) showing the full model with two MVAs with Fig. 5 b) showing the LoS-only model (i.e., $K=1$): Fused CSI performs *robustly* in resorting to estimated CSI or predicted CSI if it significantly outperforms

⁷Note that $G = P_r/P_t$ is the ratio of receive power P_r to transmit power P_t .

⁸Actually $0 < \text{SNR}/(1+\text{SNR}) < 1$ is a multiplicative gain.

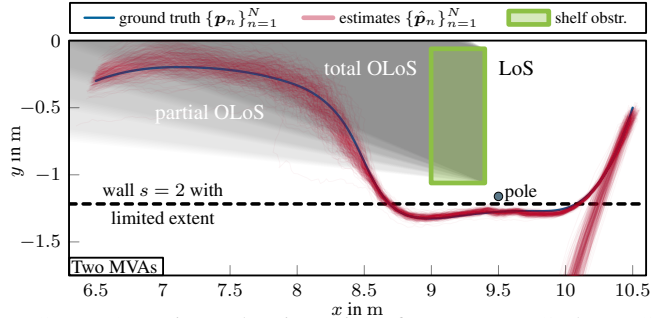


FIGURE 3: Estimated trajectories of 300 Monte Carlo (MC) estimation runs versus the true trajectory.

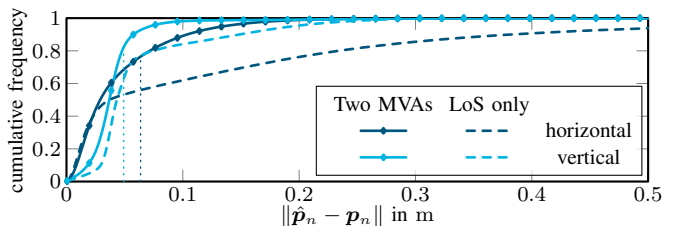


FIGURE 4: Cumulative frequency of the error of MMSE estimates w.r.t. the ground truth for all time instances n .

the respective other,⁹ e.g., during convergence in Fig. 5 a). Fused CSI gains *efficiency* if both types of estimated CSI and predicted CSI show comparable performance, as can be observed in the case of the model mismatch in Fig. 5 b). Under device *mobility*, CSI ages from one time step to the next which materializes as another significant loss incurred by a reciprocity-beamformer given outdated CSI (—). This contrasts with a geometry-based beamformer given future predicted CSI, i.e., first predicting the future state using (18) and using it to predict future CSI through (31), resulting in only a marginal efficiency loss (—).

VIII. CONCLUSIONS

In the inverse problem, we used a direct SLAM approach to infer the agent position and environment map on the uplink. In the forward problem, we used the inferred parameters to predict CSI on the downlink. Answering on our hypotheses formulated in Sec. II, we draw the following conclusions:

- 1 **Robustness:** We achieved both robust positioning in the inverse problem (see Fig. 4), and robust beamforming in the forward problem (see Fig. 5 a) by exploiting NLoS paths to bypass OLoS conditions.
- 2 **Efficiency:** Indeed, predicted CSI can outperform estimated CSI under i) low SNR. Fused CSI outperformed the other two *only* if their performance was of a similar order of magnitude in efficiency.
- 3 **Mobility Support:** Another practically relevant use for CSI prediction is ii) user mobility, where estimated CSI suffers significant losses due to CSI aging whereas CSI predicted to future time steps incurs only a marginal loss.

⁹In such regimes, fused CSI incurs a small loss w.r.t. the respective outperforming CSI.

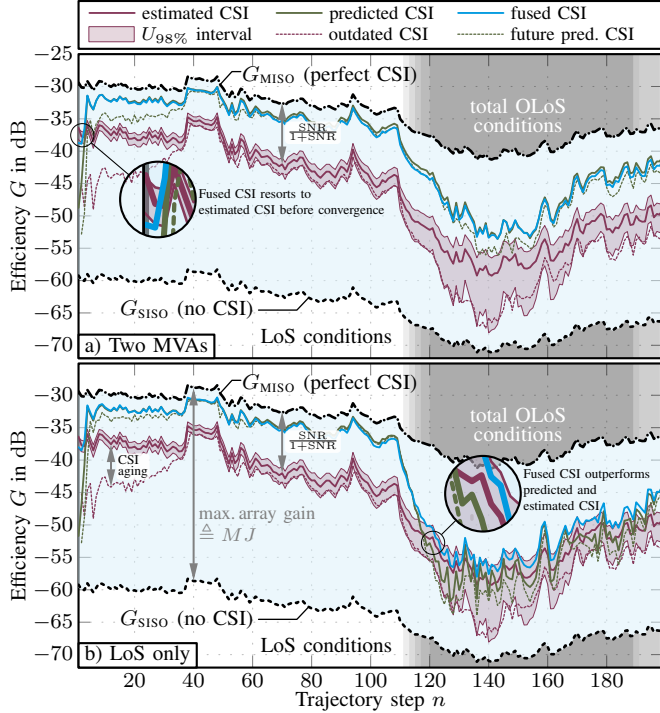


FIGURE 5: Mean efficiencies G of a conjugate beamformer given estimated CSI $\hat{\mathbf{h}}_n$, predicted CSI $\tilde{\mathbf{h}}_n$, or fused CSI \mathbf{h}_n^f .

Appendix

A. Unbiasedness

We demonstrate that our ML estimators concentrating the stochastic likelihood function in (26) from Sec. B are unbiased. Per (6), using the statistical model from Sec. B it is clear that $\mathbb{E}(\mathbf{z}_n^{(j)}|\boldsymbol{\theta}_n) = \mathbb{E}(\boldsymbol{\Psi}_j \boldsymbol{\alpha}_{n,j} + \mathbf{w}_n^{(j)}) = \boldsymbol{\Psi}_j \boldsymbol{\mu}_{n,j}$ and

$$\begin{aligned} \mathbb{E}(\mathbf{z}_n^{(j)} \mathbf{z}_n^{(j)H} | \boldsymbol{\theta}_n) &= \mathbb{E}(\boldsymbol{\Psi}_j \boldsymbol{\alpha}_{n,j} \boldsymbol{\alpha}_{n,j}^H \boldsymbol{\Psi}_j^H + \boldsymbol{\Psi}_j \boldsymbol{\alpha}_{n,j} \mathbf{w}_n^{(j)H} \\ &\quad + \mathbf{w}_n^{(j)} \boldsymbol{\alpha}_{n,j}^H \boldsymbol{\Psi}_j^H + \mathbf{w}_n^{(j)} \mathbf{w}_n^{(j)H}) \quad (35) \\ &= \boldsymbol{\Psi}_j \underbrace{\mathbb{E}(\boldsymbol{\alpha}_{n,j} \boldsymbol{\alpha}_{n,j}^H)}_{\triangleq \mathbf{P}_{n,j}} \boldsymbol{\Psi}_j^H + \underbrace{\mathbb{E}(\mathbf{w}_n^{(j)} \mathbf{w}_n^{(j)H})}_{\triangleq \sigma_j^2 \mathbf{I}_{N_f M}} \end{aligned}$$

satisfying $\mathbf{z}_n^{(j)} | \boldsymbol{\theta}_n \sim \mathcal{CN}(\boldsymbol{\Psi}_j(\boldsymbol{\theta}_n) \boldsymbol{\mu}_{n,j}, \mathbf{R}_{n,j})$. Our amplitude mean estimator in (27) is unbiased as its expectation

$$\mathbb{E}(\hat{\boldsymbol{\alpha}}_{n,j} | \boldsymbol{\theta}_n) = \boldsymbol{\Psi}_j^\dagger \mathbb{E}(\mathbf{z}_n^{(j)}) = \boldsymbol{\Psi}_j^\dagger \boldsymbol{\Psi}_j \boldsymbol{\mu}_{n,j} = \boldsymbol{\mu}_{n,j} \quad (36)$$

is the amplitude mean. Using $\boldsymbol{\Pi}_j^\perp \mathbb{E}(\mathbf{z}_n^{(j)} \mathbf{z}_n^{(j)H}) = (\mathbf{I} - \boldsymbol{\Pi}_j^\parallel) \mathbf{R}_{n,j} = \sigma_j^2 \mathbf{I} - \sigma_j^2 \boldsymbol{\Pi}_j^\parallel$, with the parallel projector $\boldsymbol{\Pi}_j^\parallel = \boldsymbol{\Psi}_j \boldsymbol{\Psi}_j^\dagger$, the noise variance estimator in (28) is unbiased as its expectation is

$$\begin{aligned} \mathbb{E}(\hat{\sigma}_j^2 | \boldsymbol{\theta}_n) &= \frac{1}{N_f M - K} \text{tr}(\sigma_j^2 \mathbf{I}_{N_f M} - \sigma_j^2 \boldsymbol{\Psi}_j \boldsymbol{\Psi}_j^\dagger) \\ &= \frac{1}{N_f M - K} (\text{tr}(\sigma_j^2 \mathbf{I}_{N_f M}) - \text{tr}(\sigma_j^2 \boldsymbol{\Psi}_j \boldsymbol{\Psi}_j^\dagger)) \\ &= \frac{1}{N_f M - K} (\sigma_j^2 \text{tr}(\mathbf{I}_{N_f M}) - \sigma_j^2 \text{tr}(\mathbf{I}_K)) \\ &= \frac{\sigma_j^2 N_f M - \sigma_j^2 K}{N_f M - K} = \sigma_j^2. \quad (37) \end{aligned}$$

Using this result, our source covariance estimator in (29) is unbiased as its expectation is

$$\begin{aligned} \mathbb{E}(\hat{\mathbf{P}}_{n,j} | \boldsymbol{\theta}_n) &= \boldsymbol{\Psi}_j^\dagger \left(\mathbb{E}(\mathbf{z}_n^{(j)} \mathbf{z}_n^{(j)H}) - \mathbb{E}(\hat{\sigma}_j^2) \mathbf{I}_{N_f M} \right) \boldsymbol{\Psi}_j^H \\ &= \boldsymbol{\Psi}_j^\dagger \left(\boldsymbol{\Psi}_j \mathbf{P}_{n,j} \boldsymbol{\Psi}_j^H + \hat{\sigma}_j^2 \mathbf{I}_{N_f M} - \hat{\sigma}_j^2 \mathbf{I}_{N_f M} \right) \boldsymbol{\Psi}_j^H \\ &= \boldsymbol{\Psi}_j^\dagger \boldsymbol{\Psi}_j \mathbf{P}_{n,j} (\boldsymbol{\Psi}_j^\dagger \boldsymbol{\Psi}_j)^H = \mathbf{P}_{n,j}. \quad (38) \end{aligned}$$

B. LMMSE Channel Estimator

Dropping indices $\{n, j\}$ for brevity, we use the identity $(\mathbf{A}^{-1} + \mathbf{B}^{-1})^{-1} = \mathbf{B}(\mathbf{A} + \mathbf{B})^{-1} \mathbf{A}$ to manipulate (33) as

$$\begin{aligned} \mathbf{h}^f &= (\mathbf{R}_m^{-1} + \mathbf{R}_p^{-1})^{-1} (\mathbf{R}_m^{-1} \tilde{\mathbf{h}} + \mathbf{R}_p^{-1} \mathbf{h}^p) \\ &= \mathbf{R}_p (\mathbf{R}_m + \mathbf{R}_p)^{-1} \mathbf{R}_m (\mathbf{R}_m^{-1} \tilde{\mathbf{h}} + \mathbf{R}_p^{-1} \mathbf{h}^p) \\ &= \mathbf{R}_p (\mathbf{R}_m + \mathbf{R}_p)^{-1} \mathbf{R}_m (\mathbf{R}_m^{-1} \tilde{\mathbf{h}} + \mathbf{R}_m^{-1} (\mathbf{h}^p - \mathbf{h}^p) + \mathbf{R}_p^{-1} \mathbf{h}^p) \\ &= \mathbf{R}_p (\mathbf{R}_m + \mathbf{R}_p)^{-1} (\tilde{\mathbf{h}} - \mathbf{h}^p) \\ &\quad + \underbrace{\mathbf{R}_p (\mathbf{R}_m + \mathbf{R}_p)^{-1} \mathbf{R}_m (\mathbf{R}_m^{-1} + \mathbf{R}_p^{-1})}_{=(\mathbf{R}_m^{-1} + \mathbf{R}_p^{-1})^{-1}} \mathbf{h}^p \\ &= \mathbf{h}^p + \mathbf{R}_p (\mathbf{R}_m + \mathbf{R}_p)^{-1} (\tilde{\mathbf{h}} - \mathbf{h}^p) \quad (39) \end{aligned}$$

showing that it is indeed equivalent to the LMMSE channel estimator in (34).

C. Efficient Implementation

The trace term in (24) and (28) involving a computationally expensive product of two $(N_f M \times N_f M)$ matrices can be simplified as

$$\begin{aligned} \text{tr}(\boldsymbol{\Pi}_j^\perp \hat{\mathbf{R}}_{n,j}^e) &= \text{tr}((\mathbf{I}_{N_f M} - \boldsymbol{\Psi}_j \boldsymbol{\Psi}_j^\dagger) \mathbf{z}_n^{(j)} \mathbf{z}_n^{(j)H}) \\ &= \text{tr}(\mathbf{z}_n^{(j)} \mathbf{z}_n^{(j)H}) - \text{tr}(\boldsymbol{\Psi}_j \boldsymbol{\Psi}_j^\dagger \mathbf{z}_n^{(j)} \mathbf{z}_n^{(j)H}) \\ &= \mathbf{z}_n^{(j)H} \mathbf{z}_n^{(j)} - \text{tr}(\boldsymbol{\Psi}_j^\dagger \mathbf{z}_n^{(j)} \mathbf{z}_n^{(j)H} \boldsymbol{\Psi}_j) \\ &= \|\mathbf{z}_n^{(j)}\|^2 - (\mathbf{z}_n^{(j)H} \boldsymbol{\Psi}_j) (\boldsymbol{\Psi}_j^\dagger \mathbf{z}_n^{(j)}) \quad (40) \end{aligned}$$

involving two less expensive matrix-vector products.

Using Sylvester's determinant theorem [46, eq.(B.1.16)] $|\mathbf{I}_N + \mathbf{A}\mathbf{B}| = |\mathbf{I}_K + \mathbf{B}\mathbf{A}|$ for matrices $\mathbf{A} \in \mathbb{C}^{N \times K}$ and $\mathbf{B} \in \mathbb{C}^{K \times N}$ as well as $|c\mathbf{X}| = c^N |\mathbf{X}|$ for $\mathbf{X} \in \mathbb{C}^{N \times N}$, the computationally expensive determinant of the $(N_f M \times N_f M)$ -matrix $\hat{\mathbf{R}}_{n,j}$ in (30) can be computed as

$$\begin{aligned} |\hat{\mathbf{R}}_{n,j}| &= \left| \hat{\sigma}_j^2 \mathbf{I}_N + \boldsymbol{\Psi}_j \hat{\mathbf{P}}_{n,j} \boldsymbol{\Psi}_j^H \right| \\ &= \hat{\sigma}_j^{2N_f M} \left| \mathbf{I}_{N_f M} + \frac{1}{\hat{\sigma}_j^2} \boldsymbol{\Psi}_j \hat{\mathbf{P}}_{n,j} \boldsymbol{\Psi}_j^H \right| \\ &= \hat{\sigma}_j^{2N_f M} \left| \mathbf{I}_K + \frac{1}{\hat{\sigma}_j^2} \hat{\mathbf{P}}_{n,j} \boldsymbol{\Psi}_j^H \boldsymbol{\Psi}_j \right| \quad (41) \end{aligned}$$

reducing to the computationally more efficient determinant of a $(K \times K)$ -matrix. Further, leveraging the Woodbury identity (inversion lemma), we likewise reduce the costly inversion

$$\begin{aligned} \mathbf{R}_{n,j}^{-1} &= \left(\hat{\sigma}_j^2 \mathbf{I}_{N_f M} + \boldsymbol{\Psi}_j \hat{\mathbf{P}}_{n,j} \boldsymbol{\Psi}_j^H \right)^{-1} \\ &= \frac{1}{\hat{\sigma}_j^2} \mathbf{I}_{N_f M} - \frac{1}{\hat{\sigma}_j^4} \boldsymbol{\Psi}_j \left(\hat{\mathbf{P}}_{n,j}^{-1} + \frac{1}{\hat{\sigma}_j^2} \boldsymbol{\Psi}_j^H \boldsymbol{\Psi}_j \right)^{-1} \boldsymbol{\Psi}_j^H \quad (42) \end{aligned}$$

to two $(K \times K)$ -matrix inversions.

REFERENCES

- [1] J. Flordelis et al, "Massive MIMO performance—TDD versus FDD: What do measurements say?" *IEEE Trans. Wireless Commun.*, vol. 17, no. 4, pp. 2247–2261, 2018.
- [2] N. Palleit and T. Weber, "Time prediction of non flat fading channels," in *2011 IEEE International Conference on Acoustics, Speech and Signal Processing (ICASSP)*, 2011, pp. 2752–2755.
- [3] D. Löschenbrand, M. Hofer, and T. Zemen, "Spectral efficiency of time-variant massive MIMO using Wiener prediction," *IEEE Wireless Commun. Lett.*, vol. 27, no. 4, pp. 1225–1229, 2023.
- [4] M. Arnold, S. Dörner, S. Cammerer, J. Hoydis, and S. ten Brink, "Towards practical FDD massive MIMO: CSI extrapolation driven by deep learning and actual channel measurements," in *2019 53rd Asilomar Conference on Signals, Systems, and Computers*, 2019, pp. 1972–1976.
- [5] A. Richter, "Estimation of radio channel parameters: Models and algorithms," Ph.D. dissertation, Technische Universität Ilmenau, Germany, February 2005.
- [6] H.-A. Loeliger, "An introduction to factor graphs," *IEEE Signal Process. Mag.*, vol. 21, no. 1, pp. 28–41, 2004.
- [7] T. L. Marzetta, E. G. Larsson, H. Yang, and H. Q. Ngo, *Fundamentals of Massive MIMO*. Cambridge University Press, 2016.
- [8] C. M. Bishop, *Pattern Recognition and Machine Learning*, 1st ed., ser. Information Science and Statistics. New York, NY: Springer, 2006.
- [9] E. G. Larsson and Y. Selen, "Linear regression with a sparse parameter vector," *IEEE Trans. Signal Process.*, vol. 55, no. 2, pp. 451–460, 2007.
- [10] O. Özdogan, E. Björnson, and E. G. Larsson, "Massive MIMO with spatially correlated Rician fading channels," *IEEE Trans. Commun.*, vol. 67, no. 5, pp. 3234–3250, 2019.
- [11] S. Kashyap, C. Mollén, E. Björnson, and E. G. Larsson, "Performance analysis of (TDD) massive MIMO with Kalman channel prediction," in *2017 IEEE International Conference on Acoustics, Speech and Signal Processing (ICASSP)*, 2017, pp. 3554–3558.
- [12] H. Kim, S. Kim, H. Lee, C. Jang, Y. Choi, and J. Choi, "Massive MIMO channel prediction: Kalman filtering vs. machine learning," *IEEE Trans. Commun.*, vol. 69, no. 1, pp. 518–528, 2021.
- [13] A. R. L. Paiva, W. C. Freitas, R. P. Antonioli, Y. C. B. Silva, and G. Fodor, "Mitigating the impact of channel aging in cell-free MIMO systems using a channel predictor based on extended Kalman filter," *IEEE Trans. Veh. Commun.*, pp. 1–17, 2025.
- [14] S. S. Thoota, J. Vieira, and E. G. Larsson, "Data-driven robust beamforming for initial access," in *GLOBECOM 2023 - 2023 IEEE Global Communications Conference*, 2023, pp. 5757–5762.
- [15] V. Rizzello, B. Böck, M. Joham, and W. Utschick, "Reverse ordering techniques for attention-based channel prediction," *IEEE Open Journal of Signal Processing*, vol. 5, pp. 248–256, 2024.
- [16] D. Neumann, T. Wiese, and W. Utschick, "Learning the MMSE channel estimator," *IEEE Trans. Signal Process.*, vol. 66, no. 11, pp. 2905–2917, 2018.
- [17] B. Fesl, M. Baur, F. Strasser, M. Joham, and W. Utschick, "Diffusion-based generative prior for low-complexity MIMO channel estimation," *IEEE Wireless Commun. Lett.*, vol. 13, no. 12, pp. 3493–3497, 2024.
- [18] M. Liang, E. Leitinger, and F. Meyer, "A belief propagation approach for direct multipath-based SLAM," in *Proc. Asilomar-23*, Pacific Grove, CA, USA, Nov. 2023.
- [19] —, "Direct multipath-based SLAM," *IEEE Trans. Signal Process.*, 2025.
- [20] T. L. Hansen, M. A. Badiu, B. H. Fleury, and B. D. Rao, "A sparse Bayesian learning algorithm with dictionary parameter estimation," in *Proc. IEEE SAM 2014*, Jun. 2014, pp. 385–388.
- [21] T. L. Hansen, B. H. Fleury, and B. D. Rao, "Superfast line spectral estimation," *IEEE Trans. Signal Process.*, vol. PP, no. 99, pp. 1–1, Feb. 2018.
- [22] S. Grebien, E. Leitinger, K. Witrisal, and B. H. Fleury, "Super-resolution estimation of UWB channels including the dense component – An SBL-inspired approach," *IEEE Trans. Wireless Commun.*, vol. 23, no. 8, pp. 10 301–10 318, Feb. 2024.
- [23] J. Möderl, F. Pernkopf, K. Witrisal, and E. Leitinger, "Variational inference of structured line spectra exploiting group-sparsity," *IEEE Trans. Signal Process.*, Nov. 2024.
- [24] J. Möderl, A. M. Westerkam, A. Venus, and E. Leitinger, "A block-sparse Bayesian learning algorithm with dictionary parameter estimation for multi-sensor data fusion," 2025. [Online]. Available: <https://arxiv.org/abs/2503.12913>
- [25] C. Gentner, W. Jost, T. and Wang, S. Zhang, A. Dammann, and U. C. Fiebig, "Multipath assisted positioning with simultaneous localization and mapping," *IEEE Trans. Wireless Commun.*, vol. 15, no. 9, pp. 6104–6117, Sept. 2016.
- [26] E. Leitinger, F. Meyer, F. Hlawatsch, K. Witrisal, F. Tufvesson, and M. Z. Win, "A belief propagation algorithm for multipath-based SLAM," *IEEE Trans. Wireless Commun.*, vol. 18, no. 12, pp. 5613–5629, Dec. 2019.
- [27] H. Kim, K. Granström, L. Gao, G. Battistelli, S. Kim, and H. Wymeersch, "5G mmWave cooperative positioning and mapping using multi-model PHD filter and map fusion," *IEEE Trans. Wireless Commun.*, vol. 19, no. 6, pp. 3782–3795, Mar. 2020.
- [28] H. Kim, K. Granstrom, L. Svensson, S. Kim, and H. Wymeersch, "PMBM-based SLAM filters in 5G mmWave vehicular networks," *IEEE Trans. Veh. Technol.*, pp. 1–1, May 2022.
- [29] E. Leitinger, A. Venus, B. Teague, and F. Meyer, "Data fusion for multipath-based SLAM: Combining information from multiple propagation paths," *IEEE Trans. Signal Process.*, vol. 71, pp. 4011–4028, 2023.
- [30] L. E. Leitinger, Wielandner, A. Venus, and K. Witrisal, "Multipath-based SLAM for cooperative navigation and map fusion," in *Proc. Asilomar-24*, Pacific Grove, CA, USA, 2024.
- [31] X. Li, X. Cai, E. Leitinger, and F. Tufvesson, "A belief propagation algorithm for multipath-based SLAM with multiple map features: A mmwave MIMO application," in *Proc. IEEE ICC 2024*, Denver, CO, USA, June 2024, pp. 269–275.
- [32] A. Fascista et al, "Joint localization, synchronization and mapping via phase-coherent distributed arrays," *IEEE J. Sel. Topics Signal Process.*, pp. 1–16, Jan. 2025.
- [33] T. Wilding, B. J. B. Deutschmann, C. Nelson, X. Li, F. Tufvesson, and K. Witrisal, "Propagation modeling for physically large arrays: Measurements and multipath component visibility," in *2023 Joint European Conference on Networks and Communications & 6G Summit (EuCNC/6G Summit)*, 2023, pp. 204–209.
- [34] B. J. B. Deutschmann, T. Wilding, M. Graber, and K. Witrisal, "XL-MIMO channel modeling and prediction for wireless power transfer," in *WS10 IEEE ICC 2023 Workshop on Near-Field Localization and Communication for 6G*, Rome, Italy, May 2023.
- [35] IEEE Standards Association, "IEEE Std 802.11ax-2021," <https://ieeexplore.ieee.org/document/9442429>, IEEE, Standard, Feb. 2021.
- [36] J. Kulmer, F. Wen, N. Garcia, H. Wymeersch, and K. Witrisal, "Impact of Rough Surface Scattering on Stochastic Multipath Component Models," in *2018 IEEE 29th Annual International Symposium on Personal, Indoor and Mobile Radio Communications (PIMRC)*, 2018, pp. 1410–1416.
- [37] L. Wielandner, A. Venus, T. Wilding, and E. Leitinger, "Multipath-based SLAM for non-ideal reflective surfaces exploiting multiple-measurement data association," *J. Adv. Inf. Fusion*, vol. 18, pp. 59–77, Dec. 2023.
- [38] L. Wielandner, A. Venus, T. Wilding, K. Witrisal, and E. Leitinger, "MIMO multipath-based SLAM for non-ideal reflective surfaces," in *Proc. Fusion-2024*, Venice, Italy, Jul. 2024.
- [39] B. J. B. Deutschmann, U. Muehlmann, A. Kaplan, G. Callebaut, T. Wilding, B. Cox, L. V. der Perre, F. Tufvesson, E. G. Larsson, and K. Witrisal, "Physically large apertures for wireless power transfer: Performance and regulatory aspects," 2025. [Online]. Available: <https://arxiv.org/abs/2503.06807>
- [40] F. Gustafsson, "Particle filter theory and practice with positioning applications," *IEEE Aerosp. Electron. Syst. Mag.*, vol. 25, no. 7, pp. 53–82, Jul. 2010.
- [41] B. Deutschmann, C. Nelson, M. Henriksson, G. Marti, A. Kosasih, N. Tervo, E. Leitinger, and F. Tufvesson, "Accurate direct positioning in distributed MIMO using delay-Doppler channel measurements," in *2024 IEEE 25th International Workshop on Signal Processing Advances in Wireless Communications (SPAWC)*, 2024, pp. 606–610.
- [42] H. Krim and M. Viberg, "Two decades of array signal processing research: the parametric approach," *IEEE Signal Process. Mag.*, vol. 13, no. 4, pp. 67–94, 1996.
- [43] P. Stoica and A. Nehorai, "On the concentrated stochastic likelihood function in array signal processing," *Circuits, Systems, and Signal Processing*, vol. 14, no. 5, pp. 669–674, Sep. 1995.
- [44] K. B. Petersen and M. S. Pedersen, *The Matrix Cookbook*. Technical University of Denmark, Nov. 2012, version 2012-11-15. [Online]. Available: <http://www2.compute.dtu.dk/pubdb/pubs/3274-full.html>
- [45] S. Kay, *Fundamentals of Statistical Signal Processing: Estimation Theory*. Prentice-Hall PTR, 1993.
- [46] C. Pozrikidis, *An Introduction to Grids, Graphs, and Networks*. Oxford University Press, 2014.